

A Novel Decoupling Technique for Single-Layered Closely-Spaced Patch Antenna Arrays

Sai Radavaram¹ and Maria Pour^{2, *}

Abstract—A new technique to reduce the mutual coupling between closely-spaced, single-layered patch antenna elements is presented. The proposed design comprises an integrated novel decoupling structure to generate an out-of-phase decoupling signal to effectively lower the coupling between the elements. In addition, coplanar L-probes and interdigital filter shaped slits on the ground plane are incorporated to further improve the isolation. The realized isolation level is about 28 dB at the frequency of operation. This is a significant achievement for a single-layered low-profile structure, wherein the center-to-center element spacing is only around $0.25\lambda_0$, and more importantly, no shorting vias are used.

1. INTRODUCTION

The usage of Multiple-Input Multiple-Output (MIMO) antenna systems has exponentially grown over the past few years and is expected to rise even higher in the coming years owing to the ever-demanding requirement of high-data transmission rates. MIMO systems aid in achieving enhanced channel throughput, efficiency, and capacity [1]. However, realizing high isolation levels between closely-spaced antenna elements is one of their biggest limitations. In the literature, various techniques have been proposed to reduce the mutual coupling between the antenna elements, including Electromagnetic Bandgap (EBG) structures [2–7], Frequency Selective Surfaces (FSS) [8], Split Ring Resonator (SRR) structures [9], defected ground structures (DGS) [10–15], decoupling transmission lines [16–21], parasitic loads [22–24], shorted patch antennas using vias [25–27], metasurface-based decoupling methods [28, 29], and exploiting both the common- and the differential-modes of operation [30–32], to name a few. Despite enhancing the isolation to an appreciable extent, these techniques inherit their own setbacks such as large center-to-center element spacing of greater than half a wavelength [2–6, 9], depreciated front-to-back (f2b) ratio [10–15], minimal isolation improvement [16–18], multi-layered structures [8, 21, 28, 29], presence of higher order modes in the radiation patterns [26, 27], complicated design and fabrication processes [2–9], etc. In summary, improving the isolation by 20 dB or more comes at the expense of larger antenna profiles with complicated structures or degraded radiation characteristics.

In this article, to overcome the aforementioned drawbacks, a novel single-layered, low-profile, tightly-spaced, two-element patch antenna array with enhanced isolation is presented and investigated. The mutual coupling between the elements is substantially reduced by cancelling out its capacitive coupling signal with the aid of an out-of-phase interference signal generated by the appended decoupling microstrip line structure. Moreover, coplanar printed L-strip feed probes [33] were used to excite each element and interdigital filter shaped slits were etched on the ground plane to further reduce the element coupling, altogether realizing an isolation of 28 dB at the resonant frequency, a ~ 24 dB improvement over its SMA probe feed counterparts. This is a significant enhancement for a patch array with a small center-to-center element spacing of $\sim 0.25\lambda_0$, where λ_0 is the free-space wavelength at the frequency of

Received 2 December 2022, Accepted 11 January 2023, Scheduled 23 January 2023

* Corresponding author: Maria Pour (maria.pour@uah.edu).

¹ Department of Chemistry and Physics, TROY University, TROY, AL 36081, USA. ² Department of Electrical and Computer Engineering, The University of Alabama in Huntsville, Huntsville, AL 35899, USA.

4.765 GHz. Moreover, the antenna has a single-layered low-profile structure ($\sim 0.02\lambda_0$) with no shorting vias.

2. COUPLING REDUCTION MECHANISM

To shed light on the coupling reduction mechanism, let us first examine a conventional closely-spaced two-element antenna array, wherein only one of the elements is excited, while the other is matched with a $50\ \Omega$ load, as depicted in Fig. 1. Considering these antenna elements to be identical and well matched, represented by a two-port reciprocal network, the reflective components of the scattering matrix could ideally be assumed zero. Likewise, the tight spacing between the elements accounts for the coupling capacitance, depicted by a lumped capacitor C_c in Fig. 1 resulting in non-zero transmission coefficients. From [34], the overall scattering parameters of the coupling network in Fig. 1 could be derived as

$$[S]_{\text{couple}} = \begin{bmatrix} 0 & \omega C_c Z_0 e^{j90^\circ} \\ \omega C_c Z_0 e^{j90^\circ} & 0 \end{bmatrix} \quad (1)$$

where ω is the angular frequency; C_c denotes the coupling capacitance between the antenna elements; and Z_0 is the characteristic impedance of the antennas.

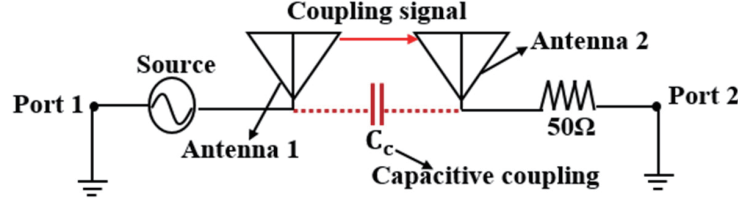


Figure 1. Schematic of a two-element array wherein only one of the elements is excited.

From (1), the signal transmitted between the antenna elements 1 and 2 has an approximate magnitude and phase shift of $\omega C_c Z_0$ and 90° , respectively. To cancel out this coupling signal, an additional decoupling/interference signal with an opposite phase shift is introduced to the system by appending a decoupling network, as illustrated in Fig. 2. This decoupling network is designed such that it potentially provides a phase shift of 270° to the signal passing through it, which will be further explained in Section 3. The scattering matrix of such a decoupling/interference signal transmitted from antenna 1 to 2 via this decoupling network can be expressed as

$$[S]_{\text{decouple}} = \begin{bmatrix} 0 & \alpha e^{j(90^\circ+180^\circ)} \\ \alpha e^{j(90^\circ+180^\circ)} & 0 \end{bmatrix} \quad (2)$$

where α is the magnitude of the interference signal. From (1) and (2), the total S -parameters of a two-element, closely-spaced antenna array with the embedded decoupling network, as shown in Fig. 2, are given as

$$[S]_{\text{total}} = [S]_{\text{couple}} + [S]_{\text{decouple}} = \begin{bmatrix} 0 & j(\omega C_c Z_0 - \alpha) \\ j(\omega C_c Z_0 - \alpha) & 0 \end{bmatrix} \quad (3)$$

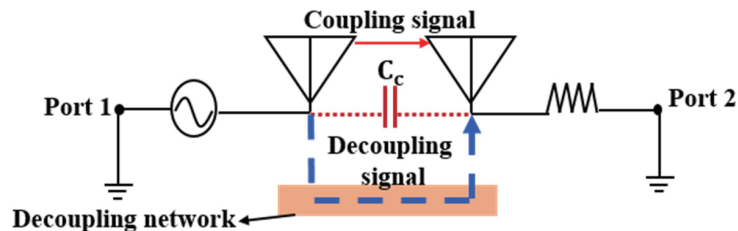


Figure 2. Schematic of a two-element array with an integrated decoupling network.

From (3), it is clear that high isolation levels are realized when the magnitude ‘ α ’ is made nearly equal to $\omega C_c Z_0$, and this could be accomplished by properly positioning and altering the parameters of the decoupling network. Further detail on their impact on the isolation levels is discussed in Section 4.

3. ANTENNA DESIGN

Based on the decoupling technique described in Section 2, the proposed antenna array is designed, as depicted in Fig. 3. The antenna comprises a low-profile grounded ($60\text{ mm} \times 60\text{ mm} \times 1.57\text{ mm}$) Rogers 5880 substrate ($\epsilon_r = 2.2$), onto which two identical rectangular patch antenna elements with dimensions of $18\text{ mm} \times 15\text{ mm}$ are printed. The center-to-center separation between these elements is only about $0.25\lambda_0$, half of the commonly used element spacing of $0.5\lambda_0$. To reduce the mutual coupling, a decoupling network comprising a pair of coupled microstrip transmission line stubs, parallel to the radiating edge of the patches, is appended near the feeding points of the antenna elements, as seen in Fig. 3(a). To further enhance the isolation, in addition to this decoupling structure, coplanar printed L-probes [33], surrounded by rectangular-shaped slots, are utilized along with incorporating interdigital filter shaped slits on the ground plane, as shown in Fig. 3(b). The positioning and the dimensions of the decoupling structure, L-strip feed, and the interdigital filter shaped slits play a vital role in realizing the desired isolation and the radiation characteristics. Thus, these parameters are numerically finalized using the Finite-Element EM solver HFSS [35], and the optimal values are given in the caption of Fig. 3.

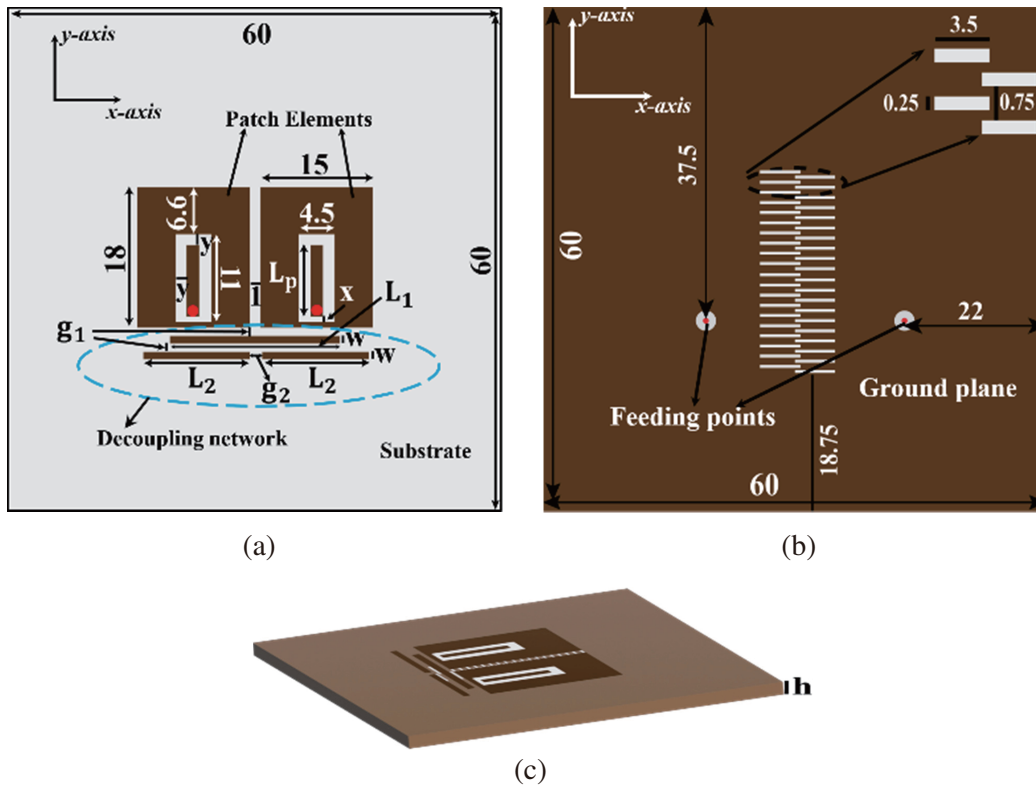


Figure 3. Geometry of the proposed antenna: (a) top view, (b) bottom view, (c) 3D transparent view. $L_1 = 23$, $L_2 = 14.1$, $g_1 = 0.5$, $g_2 = 0.8$, $w = 0.5$, $L_p = 9$, $y = 1.5$, $x = 0.5$, $h = 1.57$. All values listed here as well as in figures are in mm.

Prior to discussing the evolution of the proposed antenna structure shown in Fig. 3, it is worth explicating how the decoupling network could generate the required phase shift of 270° to the signal passing through it. To this end, an equivalent simplified circuit model of the design, shown in Fig. 4, is considered and analyzed. As observed, the interference signal originating from patch 1 couples to

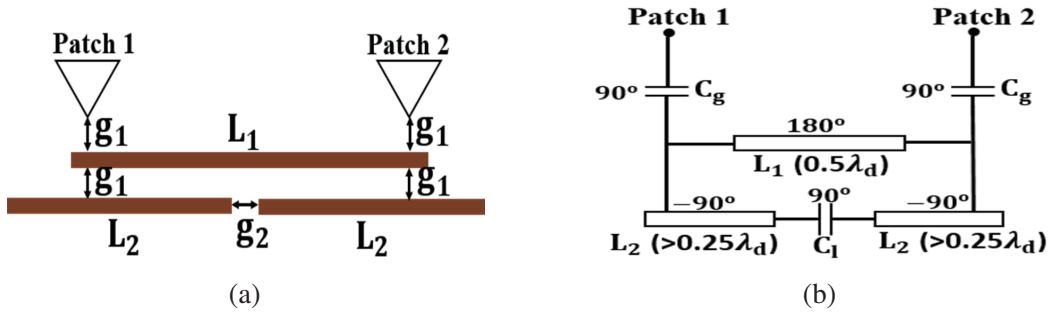


Figure 4. (a) Schematic of decoupling structure, (b) its equivalent circuit model.

the decoupling network via the capacitive gap (g_1), transmits through the network, and then couples to patch 2 via the other capacitive gap (g_1). These two capacitive gaps could ideally be replaced by lumped capacitors (C_g), as shown in Fig. 4(b). These capacitors add nearly 90° phase shift each, a total of 180° phase shift. The microstrip line (L_1) of the decoupling network is approximately $\lambda_d/2$ in length, where λ_d is the dielectric wavelength at the frequency of operation, thus generating a 180° phase shift at the resonant frequency. On the other hand, each of the microstrip lines, labelled L_2 , is slightly longer than $\lambda_d/4$. From the transmission line analysis, an open-ended line with the length greater than $\lambda_d/4$ acts as an inductor, causing a phase delay of 90° . Thus, these two lines (L_2) create a total phase lag of 180° . The capacitive gap (g_2) between the lines (L_2), modeled by a lumped capacitor C_l in Fig. 4(b), adds another 90° phase shift to the signal at the resonant frequency. Hence, the total phase shift experienced by the signal transmitting from patch 1 to patch 2 via these decoupling transmission lines is approximately 270° .

For further clarification, the evolution of the design and its S -parameters at each phase of the design are depicted in Fig. 5. As observed, when the tightly-spaced antenna elements are fed using the conventional SMA probe feeds (Antenna 1), the levels of the mutual coupling are as high as -4 dB at the resonating frequency of 4.93 GHz. Appending the decoupling network to this design (Antenna 2) resulted in improving the isolation to ~ 17 dB at the resonant frequency, a 13 dB improvement over the conventional case. It is noticed that the resonating frequency is now shifted down to ~ 4.6 GHz. This is owing to the fact that incorporating the decoupling structure results in increasing the overall resonant length of the antenna. To further improve the isolation beyond 17 dB, coplanar L-probe feeds adopted from [33], surrounded by rectangular shaped slots, are used to excite the patches (Antenna 3). These slots facilitated in capacitively feeding the elements in lieu of directly feeding them, thereby aiding in increasing the isolation by another ~ 6 dB, as noticed in Fig. 5(c). Finally, to further enhance the isolation, right underneath the middle of the radiating patches, interdigital filter shaped slits, in total of 40, are symmetrically etched on the ground plane, as shown in Fig. 3(b). With the incorporated decoupling transmission lines, L-strip feeds, and the interdigital filter shaped slits, an isolation of ~ 30 dB is achieved at the resonating frequency of 4.765 GHz, per Fig. 5(c). Overall, a 26 dB improvement is realized compared to the conventional case, which is quite significant for such a low-profile single-layered structure with a small center-to-center element spacing of $\sim 0.25\lambda_0$. The concept also works for an asymmetric antenna structure. For example, for a 5 mm-displacement along the y -axis, the isolation level is about 29 dB, which is still quite significant. The Envelope Correlation Coefficient (ECC) is also calculated using the complex far-field radiation patterns of the antenna elements, per [36], for both the cases of conventional SMA probe fed antenna elements (Antenna 1) and the proposed antenna structure. They are plotted along with their S -parameters in Figs. 5(d) and 5(e), respectively. As observed, at the resonating frequencies, the ECC is as high as ‘0.4’ for the conventional case, whereas, it is near ‘0’ for the proposed technique. This further validates the isolation enhancement with the proposed decoupling technique.

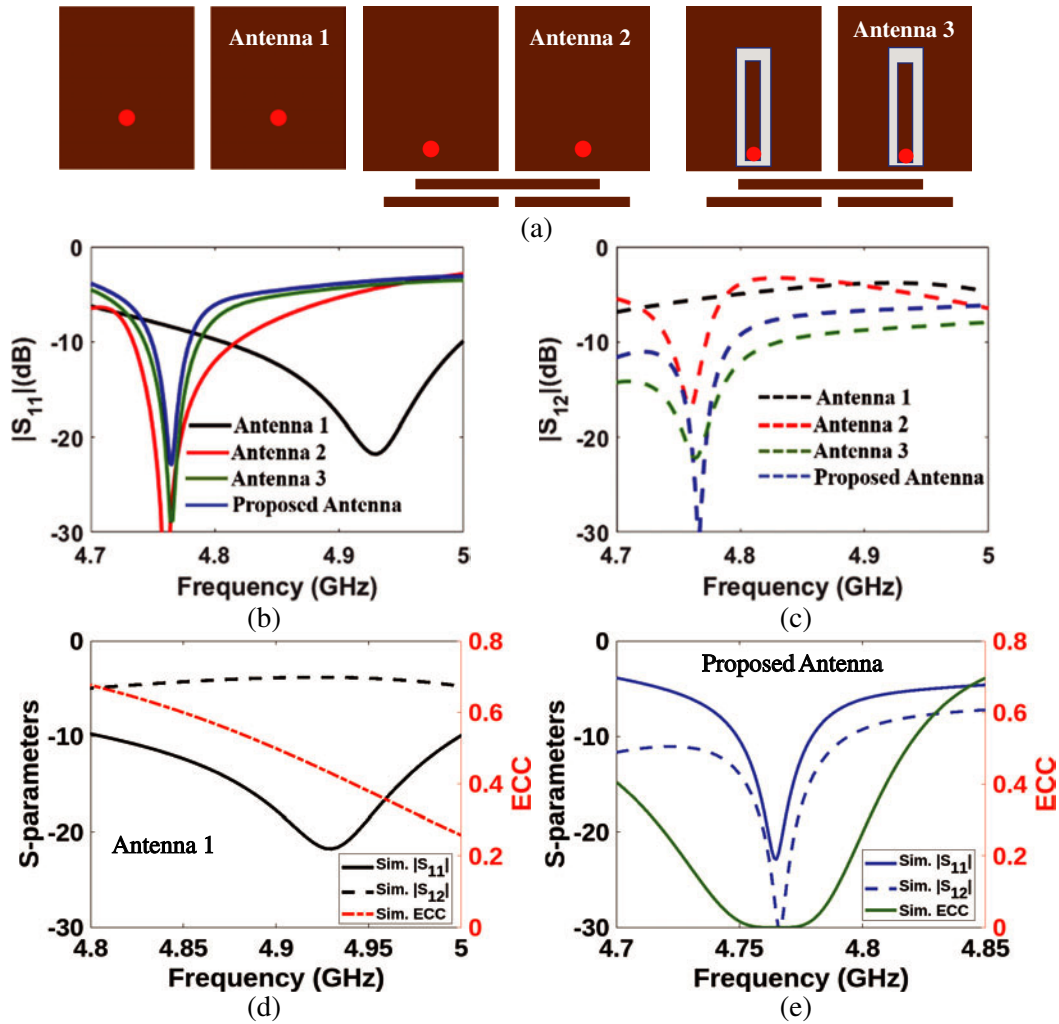


Figure 5. (a) Evolution of the proposed antenna design, (b) & (c) equivalent S -parameters at each stage (d) & (e) Overlaid S -parameters and ECC of antenna 1 and proposed antenna, respectively.

4. PARAMETRIC INVESTIGATION

From Fig. 3, it is observed that the proposed antenna design possesses a handful of parameters. However, not all the parameters have an effective impact on the isolation, and thus the discussion here is limited to the non-trivial parameters, i.e., the parameters of decoupling network, L-strip feed, and the interdigital filter shaped slits. As for the decoupling network, the lengths of the microstrip lines are effectively chosen to provide a phase shift of 270° to the interference signal passing through it. In addition to this desired phase shift, the magnitude of the decoupling signal also plays a vital role in the effective reduction of mutual coupling, per (3). This magnitude is mainly altered by the decoupling network parameters ‘ g_1 ’, ‘ g_2 ’, and ‘ w ’ of Fig. 3. To investigate their impact on the impedance characteristics, each of these parameters is varied independently by keeping the rest of the antenna parameters unchanged, and the respective S -parameters are plotted in Fig. 6. The variation of g_1 and g_2 had more or less a similar impact on the isolation. The isolation deteriorates as the value of g_1 or g_2 increases. The much larger values of g_1 or g_2 result in altogether losing the impact of the decoupling structure on the isolation, as noticed in Figs. 6(a) and 6(b). The isolation of ~ 30 dB is realized with the values of g_1 and g_2 as 0.5 mm and 0.8 mm, respectively. On the other hand, increasing the width of the transmission lines (w) effectively increases the overall resonating length of the antenna, and thereby pushing the resonating

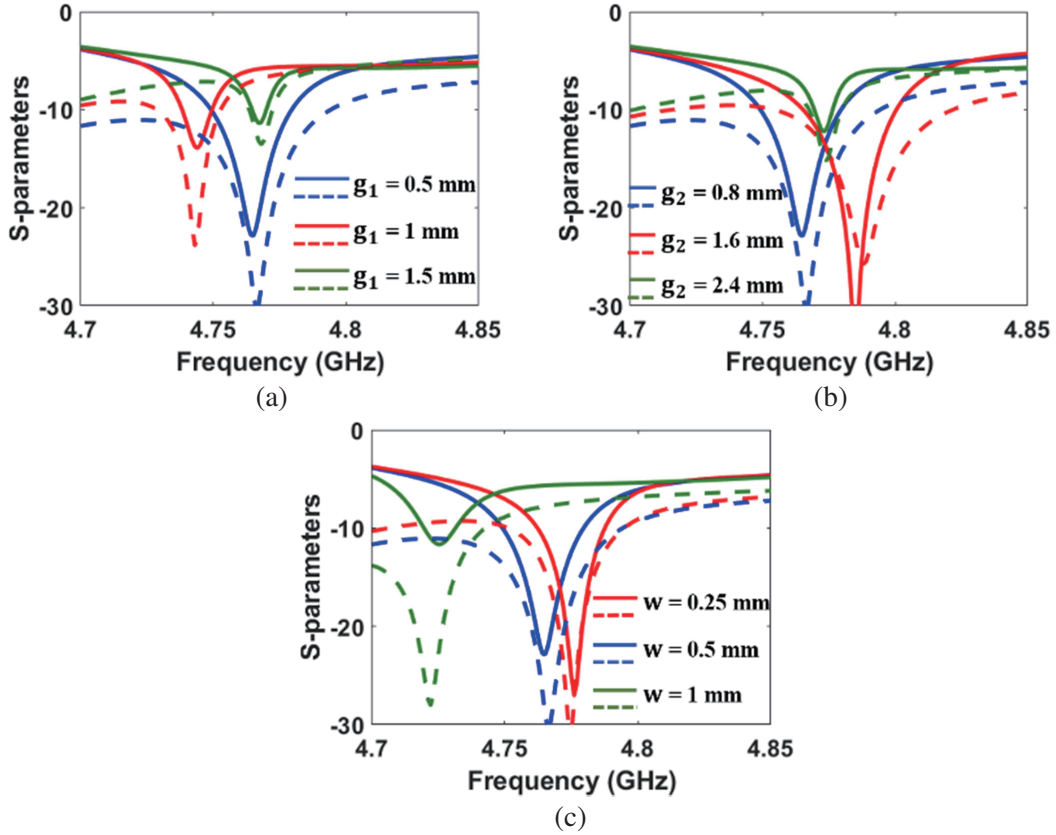


Figure 6. Impact of the decoupling network variables on the S -parameters. (a) ‘ g_1 ’, (b) ‘ g_2 ’, and (c) ‘ w ’. In all these figures, solid lines represent $|S_{11}|$ (dB) and dashed lines represent $|S_{12}|$ (dB).

frequencies towards the lower frequencies (Fig. 6(c)). As noticed, an increase in ‘ w ’ has a minor impact on the isolation. The value of ‘ w ’ is chosen as 0.5 mm instead of 0.25 mm to avoid fabrication errors.

As for the parameters of the L-strip feed, the capacitive gaps labelled ‘ x ’ and ‘ y ’ in Fig. 3(a) play a vital role in improving the isolation as compared to the length of the L-strip feed (L_p). Varying L_p largely impacts the resonant frequency of the antenna than the isolation, whose results are omitted here for brevity. From Fig. 3, it is observed that increasing the ‘ x ’ values results in pushing away the feeding points from the decoupling structure, and thus degrading the isolation, as noticed in Fig. 7(a). To study the impact of the other capacitive gap ‘ y ’, its value is varied from 1 mm to 2 mm with a step of 0.5 mm and the results are plotted in Fig. 7(b). As observed, increasing the values of ‘ y ’ enhances the isolation levels at the expense of losing the antenna impedance matching.

As seen in Fig. 3(b), on the ground plane, the interdigital filter shaped slits are symmetrically etched and stretched out right along the radiating structure of the antenna. The total number of slits and their dimensions are rightly chosen such that an improved isolation is realized, while minimally impacting the f2b ratio. The finalized slit parameters are labelled in Fig. 3. Increasing their width, length, or the gap between the slits improves the isolation levels but such larger dimensions result in further defecting the ground plane and thus diminishing the f2b ratio. These results are omitted here for brevity. It is worth mentioning that incorporating more number of slits along the entire length of the ground plane has a minimal impact on the overall isolation improvement.

5. MEASUREMENT RESULTS

The proposed closely-spaced two-element antenna array was fabricated and experimentally validated in terms of its scattering and radiation characteristics. The simulated and the measured S -parameters

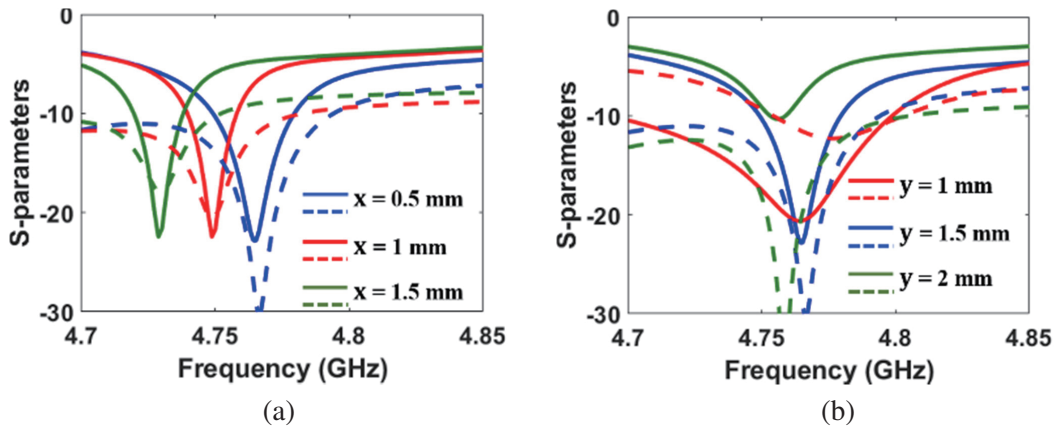


Figure 7. Impact of L-strip parameters on the impedance characteristics. (a) ‘*x*’, (b) ‘*y*’. In these figures, solid and dashed lines represent $|S_{11}|$ (dB) and $|S_{12}|$ (dB), respectively.

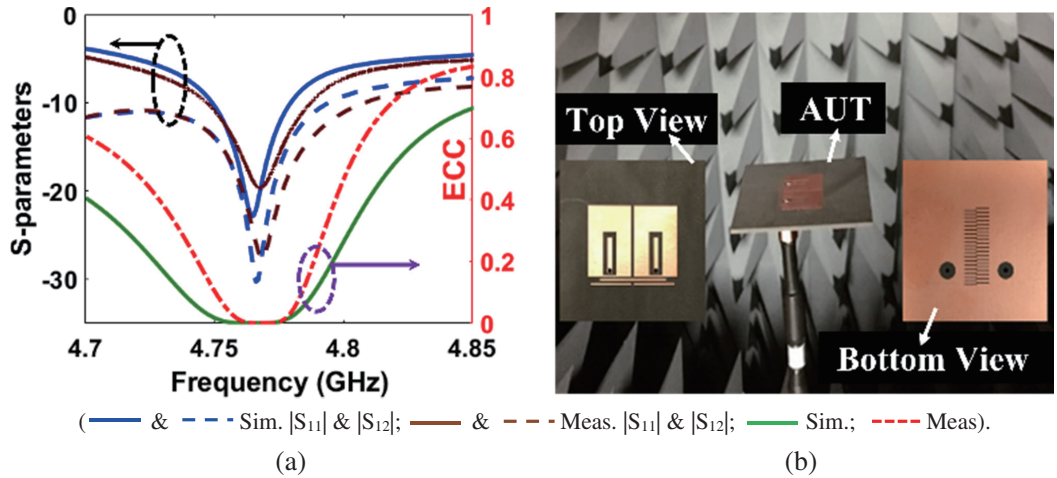


Figure 8. (a) Simulated and measured S -parameters and ECC. (b) Photographs of the fabricated prototype and AUT.

along with the ECC are plotted in Fig. 8(a). Good agreement between the simulated and the measured scattering parameters is observed and the realized isolation levels (experimental) at the resonant frequency of operation is ~ 28 dB, i.e., a ~ 24 dB improvement over the conventional case. Moreover, as noticed in Fig. 8(a), both the simulated and the measured ECC values are near zero at the operating frequency of the antenna array, thereby further validating the independency of the antenna elements. A photograph of the Antenna Under Test (AUT) and the embedded top and bottom views of the fabricated prototype are shown in Fig. 8(b).

The measured and simulated co-pol and cross-pol radiation patterns of the proposed antenna at the resonant frequency of 4.765 GHz are plotted in Fig. 9, when only one patch is excited and the other is matched with the 50Ω load. In both the E - and H -planes, the simulated and measured patterns matched quite well, with a realized boresight gain of ~ 7 dBi and a front-to-back ratio of ~ 18 dB.

To further showcase the effectiveness of the proposed antenna array in terms of its small element spacing, fabrication simplicity, low profile, and isolation improvement, its characteristics are compared with those of a few recently published single-layered decoupling antenna arrays in Table 1. As summarized, the proposed design excels the other antennas in many aspects that are ideal for MIMO applications.

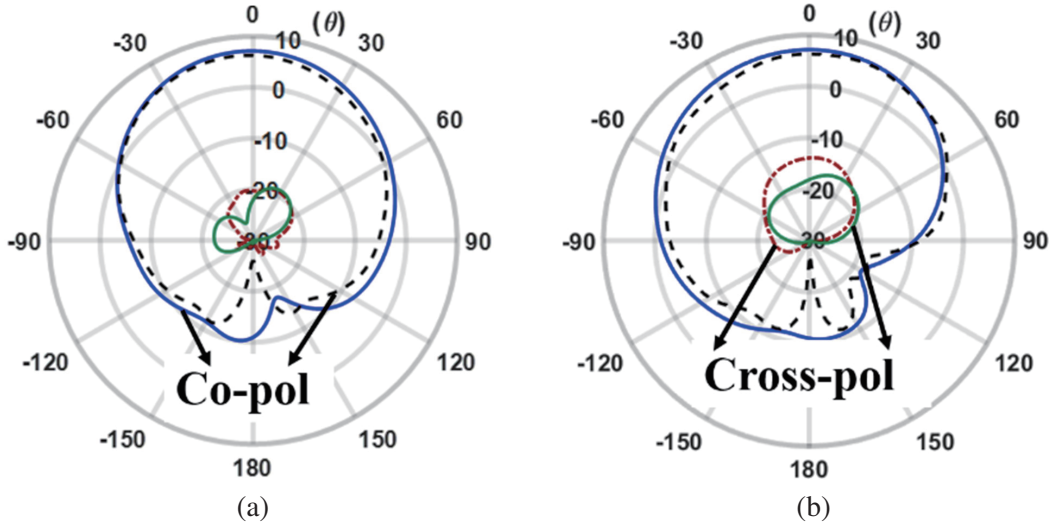


Figure 9. Simulated and measured co-pol and cross-pol patterns. (a) E -plane, (b) H -plane. The solid and dashed curves are simulated and measured results, respectively.

Table 1. Comparative study with single layered decoupling antenna arrays.

Ref.	Element spacing (λ_0)	Profile (λ_0)	Isolation improvement	f2b ratio (dB)	Single-layered design
[6]	~ 1.4	~ 0.16	~ 37 dB	NA	yes
[11]	~ 0.5	~ 0.01	~ 30 dB	8	no
[13]	~ 0.38	~ 0.01	~ 20 dB	7	yes
[15]	~ 0.5	~ 0.05	~ 9 dB	NA	yes
[21]	~ 0.5	~ 0.06	~ 25 dB	17	no
[24]	~ 0.43	~ 0.11	~ 17 dB	20	no
This work	~ 0.25	~ 0.02	~ 24 dB	18	yes

6. CONCLUSION

A novel single-layered, low-profile, closely-spaced patch antenna array with enhanced isolation is presented and investigated in this article. The measured isolation levels at the resonant frequency is ~ 28 dB, a 24 dB of improvement over the conventional case. More importantly, such isolation levels are achieved for a small element spacing of $\sim 0.25\lambda_0$. No shorting vias are used either. The proposed design was fabricated and validated for its scattering parameters and radiation characteristics. Good agreement between the measured and the simulated results was observed.

REFERENCES

1. Larsson, E. G., O. Edfors, F. Tufvesson, and T. L. Marzetta, "Massive MIMO for next generation wireless systems," *IEEE Comm. Magz.*, Vol. 52, No. 2, 186–195, Feb. 2014.
2. Yang, L., M. Fan, F. Chen, J. She, and Z. Feng, "A novel compact electromagnetic-bandgap (EBG) structure and its applications for microwave circuits," *IEEE Trans. Microw. Theory Tech.*, Vol. 53, No. 1, 183–190, Jan. 2005.

3. Yang, F. and Y. R. Samii, "Microstrip antennas integrated with electromagnetic band-gap EBG structures: A low mutual coupling design for array applications," *IEEE Trans. Antennas Propag.*, Vol. 51, No. 10, 2936–2946, Oct. 2003.
4. Farahani, H. S., M. Veysi, M. Kamyab, and A. Tadjalli, "Mutual coupling reduction in patch antenna arrays using a UC-EBG superstrate," *IEEE Antennas Wireless Propag. Lett.*, Vol. 9, 57–59, 2010.
5. Yang, X., Y. Liu, Y. Xu, and S. Gong, "Isolation enhancement in patch antenna array with fractal UC-EBG structure and cross slot," *IEEE Antennas Wireless Propag. Lett.*, Vol. 16, 2175–2178, 2017.
6. Alibakhshikenari, M., M. Khalily, B. S. Virdee, C. H. See, R. A. Abd-Alhameed, and E. Limiti, "Mutual coupling suppression between two closely placed microstrip patches using EM-bandgap metamaterial fractal loading," *IEEE Access*, Vol. 7, 23606–23614, 2019.
7. Liu, Y., X. Yang, Y. Jia, and Y. J. Guo, "A low correlation and mutual coupling MIMO antenna," *IEEE Access*, Vol. 7, 127384–127392, 2019.
8. Karimian, R., A. Kesavan, M. Nedil, and T. A. Denidni, "Low-mutual-coupling 60-GHz MIMO antenna system with frequency selective surface wall," *IEEE Antennas Wireless Propag. Lett.*, Vol. 16, 373–376, 2017.
9. Qamar, Z., L. Riaz, M. Chongcheawchamnan, S. A. Khan, and M. F. Shafique, "Slot combined complementary split ring resonators for mutual coupling suppression in microstrip phased arrays," *IET Microw., Antennas Propag.*, Vol. 8, No. 15, 1261–1267, Sep. 2014.
10. Habashi, A., J. Nourinia, and C. Ghobadi, "Mutual coupling reduction between very closely spaced patch antennas using low-profile folded split-ring resonators (FSRRs)," *IEEE Antennas Wireless Propag. Lett.*, Vol. 10, 862–865, 2011.
11. Gao, D., Z.-X. Cao, S. -D. Fu, X. Quan, and P. Chen, "A novel slot-array defected ground structure for decoupling microstrip antenna array," *IEEE Trans. Antennas Propag.*, Vol. 68, No. 10, 7027–7038, Oct. 2020.
12. Dey, S., S. Dey, and S. K. Koul, "Isolation improvement of MIMO antenna using novel ebg and hair-pin shaped DGS at 5G millimeter wave band," *IEEE Access*, Vol. 9, 162820–162834, 2021.
13. Qian, B., X. Chen, and A. A. Kishk, "Decoupling of microstrip antennas with defected ground structure using the common/differential mode theory," *IEEE Antennas Wireless Propag. Lett.*, Vol. 20, No. 5, 828–832, May 2021.
14. Govindarajulu, S. R., A. Jenkel, R. Hokayem, and E. A. Alwan, "Mutual coupling suppression in antenna arrays using meandered open stub filtering technique," *IEEE Open Jrn. Antennas Propag.*, Vol. 1, 379–386, 2020.
15. Askarian, A., J. Yao, Z. Lu, and K. Wu, "Surface-wave control technique for mutual coupling mitigation in array antenna," *IEEE Microw. Wireless Compon. Lett.*, Vol. 32, No. 6, 623–626, Jun. 2022.
16. Pei, T., L. Zhu, J. Wang, and W. Wu, "A low-profile decoupling structure for mutual coupling suppression in MIMO patch antenna," *IEEE Trans. Antennas Propag.*, Vol. 69, No. 10, 6145–6153, Oct. 2021.
17. Cheng, Y., X. Ding, W. Shao, and B. Wang, "Reduction of mutual coupling between patch antennas using a polarization-conversion isolator," *IEEE Antennas Wireless Propag. Lett.*, Vol. 16, 1257–1260, 2017.
18. Farsi, S., H. Aliakbarian, D. Schreurs, B. Nauwelaers, and G. A. E. Vandenbosch, "Mutual coupling reduction between planar antennas by using a simple microstrip U-section," *IEEE Antennas Wireless Propag. Lett.*, Vol. 11, 1501–1503, 2012.
19. Vishvaksean, K. S., K. Mithra, R. Kalaiarasan, and K. S. Raj, "Mutual coupling reduction in microstrip patch antenna arrays using parallel coupled-line resonators," *IEEE Antennas Wireless Propag. Lett.*, Vol. 16, 2146–2149, 2017.
20. Meng, H. and K.-L. Wu, "An LC decoupling network for two antennas working at low frequencies," *IEEE Trans. Microw. Theory Tech.*, Vol. 65, No. 7, 2321–2329, Jul. 2017.

21. Zhang, Y. M. and S. Zhang, "A novel aperture-loaded decoupling concept for patch antenna arrays," *IEEE Trans. Microw. Theory Tech.*, Vol. 69, No. 9, 4272–4283, Sept. 2021.
22. Lau, B. K. and J. B. Andersen, "Simple and efficient decoupling of compact arrays with parasitic scatterers," *IEEE Trans. Antennas Propag.*, Vol. 60, No. 2, 464–472, Feb. 2012.
23. Zhao, L. and K. Wu, "A decoupling technique for four-element symmetric arrays with reactively loaded dummy elements," *IEEE Trans. Antennas Propag.*, Vol. 62, No. 8, 4416–4421, Aug. 2014.
24. Zhai, G., Z. N. Chen, and X. Qing, "Mutual coupling reduction of a closely spaced four-element MIMO antenna system using discrete mushrooms," *IEEE Trans. Microw. Theory Tech.*, Vol. 64, No. 10, 3060–3067, Oct. 2016.
25. Zaker, R. and A. Kheiridoost, "Bandwidth and isolation improvement of highly coupled printed array antenna using multiple shorting posts," *IEEE Trans. Antennas Propag.*, Vol. 69, No. 11, 7987–7992, Nov. 2021.
26. Yang, W., L. Chen, S. Pan, W. Che, and Q. Xue, "Novel decoupling method based on coupling energy cancellation and its application in 5G dual-polarized high-isolation antenna array," *IEEE Trans. Antennas Propag.*, Vol. 70, No. 4, 2686–2697, Apr. 2022.
27. Liu, N.-W., L. Zhu, Z. -X. Liu, M. Li, G. Fu, and Y. Liu, "A novel low-profile circularly polarized diversity patch antenna with extremely small spacing, reduced size, and low mutual coupling," *IEEE Trans. Antennas Propag.*, Vol. 70, No. 1, 135–144, Jan. 2022.
28. Sufian, M. A., N. Hussain, H. Askari, S. G. Park, K. S. Shin, and N. Kim, "Isolation enhancement of a metasurface-based MIMO antenna using slots and shorting pins," *IEEE Access*, Vol. 9, 73533–73543, 2021.
29. Luan, H., C. Chen, W. Chen, L. Zhou, H. Zhang, and Z. Zhang, "Mutual coupling reduction of closely E/H -plane coupled antennas through metasurfaces," *IEEE Antennas Wireless Propag. Lett.*, Vol. 18, No. 10, 1996–2000, Oct. 2019.
30. Sun, L., Y. Li, Z. Zhang, and H. Wang, "Antenna decoupling by common and differential modes cancellation," *IEEE Trans. Antennas Propag.*, Vol. 69, No. 2, 672–682, Feb. 2021.
31. Sun, L., Y. Li, and Z. Zhang, "Decoupling between extremely closely spaced patch antennas by mode cancellation method," *IEEE Trans. Antennas Propag.*, Vol. 69, No. 6, 3074–3083, Jun. 2021.
32. Lai, Q. X., Y. M. Pan, S. Y. Zheng, and W. J. Yang, "Mutual coupling reduction in MIMO microstrip patch array using TM_{10} and TM_{02} modes," *IEEE Trans. Antennas Propag.*, Vol. 69, No. 11, 7562–7571, Nov. 2021.
33. Radavaram, S. and M. Pour, "A wideband coplanar L-strip fed rectangular patch antenna," *IEEE Antennas Wireless Propag. Lett.*, Vol. 20, No. 9, 1779–1783, 2021.
34. Pozar, D. M., "Microwave network analysis," *Microwave Engineering*, 4th Edition, Wiley, Hoboken, NJ, USA, 2012.
35. *High Frequency Structure Simulator (HFSS)*, ANSYS, Canonsburg, PA, USA, 2022 R1.
36. Ludwig, A., "Mutual coupling, gain and directivity of an array of two identical antennas," *IEEE Trans. Antennas Propag.*, Vol. 24, No. 6, 837–841, Nov. 1976.